Chapter 6

Qualification of PWAS-Based SHM Technology for Space Applications

Ioan Ursu, Mihai Tudose and Daniela Enciu

Additional information is available at the end of the chapter

http://dx.doi.org/10.5772/intechopen.78034

Abstract

The chapter refers to the results obtained in the framework of a national research project whose novelty was that concomitant outer space constraints, namely extreme temperature variations, radiations and vacuum, were applied to structures specimens to study their effect on the structural health monitoring (SHM) technology based on piezoelectric wafer active sensors (PWAS) and electromechanical impedance spectroscopy (EMIS) method of damages detection and identification. The results, in short, concern (a) the survivability and sustainability of EMIS technique, in fact the PWAS transducers survival, in these harsh conditions and (b) the developing of a methodology to distinguish between the damages of mechanical origin, and the false ones, caused by environmental conditions, which are, basically, harmless. This has resulted by observing that the splitting phenomenon of resonance peaks on EMIS signature can be associated with the occurrence of mechanical damage, making so possible the clear dissociation of the changes determined by the harsh environmental conditions.

Keywords: lab tests, electromechanical impedance spectroscopy (EMIS), piezoelectric wafer active sensor (PWAS), outer space harsh environmental conditions, entropy, real damage versus false damage

1. Introduction

In the beginning, we prefer to appeal to the well-known definitions. In this book chapter, "the process of implementing a damage identification strategy for aerospace, civil and mechanical engineering infrastructure is referred to as structural health monitoring (SHM). […] The damage is defined as changes to the material and/or geometric properties of these systems, including changes to the boundary conditions and system connectivity, which adversely affect the

current or future performance of these systems" [1]. SHM is, properly, an on-line measurement process supposing a sensor system distributed over the monitored structure. This process is complemented by off-line analysis of damage-sensitive features from these measurements, or by an on-line analysis of damages occurrence, as shown in this contribution. SHM technology enjoys special attention over the past two to three decades. The sensors used to damage detection belong to a wide range, such as optical fiber sensors [2, 3], acoustic active and passive sensors [4–6], microelectromechanical systems (MEMS) [7], and wireless sensor systems [8]. The basic SHM methods are the method based on a modal modification of structure dynamic vibrations in a relatively low-frequency register [9] and the electromechanical method of impedance spectroscopy (EMIS) in the high-frequency register, using the active piezo sensors [10–14]. It should be added that SHM methodology has been strongly related during its development to predictive maintenance [15] and fault detection [16] techniques due to safety demands in all areas of activity, especially in aerospace applications, chemical industry, nuclear power plants, and so on. SHM methodology has its obvious relevance to the air and space industry but has become imperious for many other industries due to the increase of the productivity and quality demands (zero-defects manufacturing), cost savings together with enhanced safety, and increased availability. Of course, not all existing damages compromise the good functioning of the structure. Based on a long-time SHM process, one obtains information on the ability of the structure to perform in spite of the inevitable aging and degradation resulting from operational environments [1], with the benefit to managing the structures life prognosis and reducing life-cycle costs. SHM will be one of the major contributions for future smart structures, including space ones [17].

2. PWAS-based SHM technology—EMIS method

The active SHM sensing techniques are based on two different approaches: transient guided waves and standing waves [12]. In such SHM processes, a piezoelectric wafer active sensor (PWAS) is required to generate elastic waves. These travel along the mechanical structure, are reflected by different structural abnormalities, or boundary edges, and they are recaptured by the same sensor in a pulse-echo configuration or by other sensors of same or different type, even passive sensors, and in pitch-catch configuration. If the structural damage or boundary edges are in the close vicinity of the active sensor, their reflections overlap the incident transient wave, and making impossible the interpretation [14]. One of the active SHM sensing techniques is based on standing waves, in the so-called EMIS method; by sweeping the frequency of the input signals to PWAS, some changes appear in the impedance measured by an impedance analyzer connected to the PWAS terminals. By monitoring the changes in the real part of the impedance function, which is most sensitive to structural changes [10], one can evaluate the integrity of the host structure.

The EMIS method uses PWAS high-frequency active sensors and bonded to the structure. The presence of damage in a neighboring zone of the sensor is signaled as its EMIS "signature," respectively, as a modification of the electromagnetic impedance spectrum Z (ω), recorded and online processed, and in principle [10–14]. The pioneering work on using EMIS

http://dx.doi.org/10.5772/intechopen.78034

in SHM technology is considered [10] (see [11]). The electromechanical impedance spectrum is defined as the ratios between the applied excitation voltage $V(t) \coloneqq V_0 \sin(\omega t)$ [V] and the current $I(t) \coloneqq I \sin(\omega t)$ [A] generated by the piezoelectric effect. Where appropriate, impedance results are obtained based on an analytical relationship, or by dedicated equipment such as the HP 4194A impedance analyzer. Experimentally it has been proven that the real part, Re (Z (ω)), of the EMIS PWAS attached to the structure can be taken as an indication of the presence of damage or defects, due to the fact that this value closely follows the resonance behavior of the structure vibrating under the PWAS excitation [11]. In other words, this measured value is very sensitive to the smallest variations in the high-frequency structural dynamics at local scales (on the order of microns), which are associated with the presence of incipient damage. Of course, these changes cannot be detected by classical modal analysis sensors operating at lower frequencies.

3. Theoretical and experimental framework of qualification PWAS based SHM technology for space applications

Although SHM will be soon, we think, a key technology in the field of space vehicles, it is surprising how few papers can be reported for the time being in this field [4, 5, 18–22]. However, it is becoming clearer that new space programs can no longer ignore the implementation of SHM technologies to monitor and test the health and performance of space structures. The safety of the crew on board and the safety of the spacecraft, especially in critical moments of launch and re-entry into the earth's atmosphere, depend on the onboard existence of a SHM system. Spatial vehicles, but also the satellites, are subject to harsh environmental conditions: strong vibrations at launching and landing, cosmic radiation (with energy up to 1.6×10^{-11} J (1 GeV) [23], extreme temperatures (+120°C for exposed surfaces to the Sun and −230°C for unexposed surfaces [22]), and advanced vacuum.

The premise of a tests program for qualification PWAS-based SHM technology for space applications is that the changes in the EMIS signature will reflect the complex conditions in which the structures are found: overexposure to natural damage, that is, mechanical fatigue and aging, and special operating conditions in an environment defined by outer space (extreme temperatures, radiation, and vacuum). Both kinds of constraints, that is, mechanical and environmental, are to be simulated. The specific problem of the tests relates to the ability of the PWAS transducer to measure the modal behavior of the structure on which it is attached in the simulated harsh environmental conditions and with simulated mechanical damages. Consequently, a considerable amount of testing stages, EMIS records, data processing, and analytical assessments on damage identification were performed [5, 6, 24–28]. The following types of specimens were subjected to the tests: (a) PWAS STEMINC SMD07T02S412WL transducers, (b) M-bond 610 Vishay epoxy adhesive, and (c) STEMINC PWAS transducers [26] (**Figure 1**). The material and geometry data of the disc specimens (DS) were: A2024 aluminum alloy, with a diameter of 100 mm and a thickness of 0.8 mm. To simulate damages, in discs were processed, with laser technology, slits with 10 mm in length and 0.15 mm width, of various geometries, and locations.

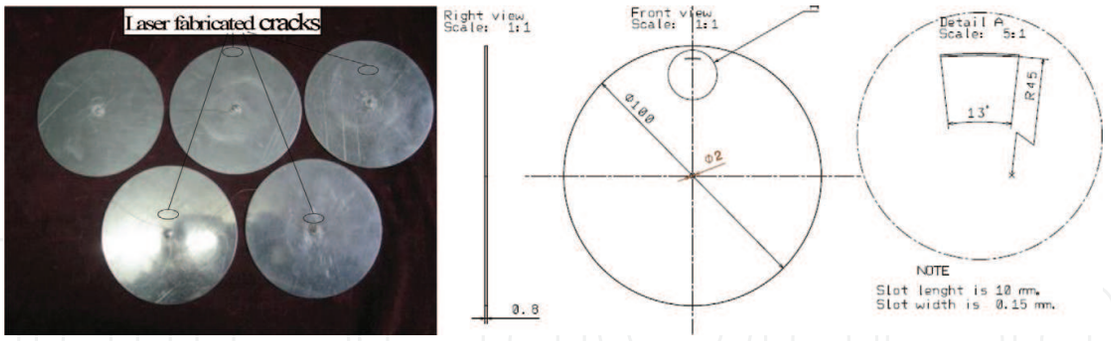

Figure 1. Disc specimens (DS), geometry of damage simulation.

Disc type PWASs with a diameter of 8 mm was bonded in the center of the aluminum disc specimen with epoxy adhesive. The thickness of the adhesive layer was measured with a comparator, and was found to be between 20 and 100 μm. **Figure 2** shows a disc with an arc-type simulated crack damage at 7 mm from the PWAS. The geometry of the simulated cracks (0.15 mm wide and 10 mm long) is the following: crack 1 (curvature):R = 45 mm, θ = 13°; crack 2:R= 25 mm, θ = 23°; crack 3: R = 15 mm, θ=38°; and crack 4: R = 7 mm, θ = 82°. The set of records refer to either PWASs or specimens with bonded PWAS, without and with simulated damages. In **Figure 2c**, the experimental set-up for EMIS recording using the HP 4194A impedance analyzer is presented.

The SHM test protocol involved a lot of operations: records and processing for EMIS, extreme temperature irradiation under high-vacuum, irradiation at room temperature (RT) and atmospheric pressure, optical and acoustic microscopy, scanning laser Doppler vibrometry (SLDV). From the processing of impedance spectrum will result in the characterization of damages. This is done by scalar sizes suitable to capture the differences between the spectra caused by this damage/crack. Ideally, these values should capture only those spectral features that are directly altered by the damage, while the variations caused by normal operating conditions to be neglected.

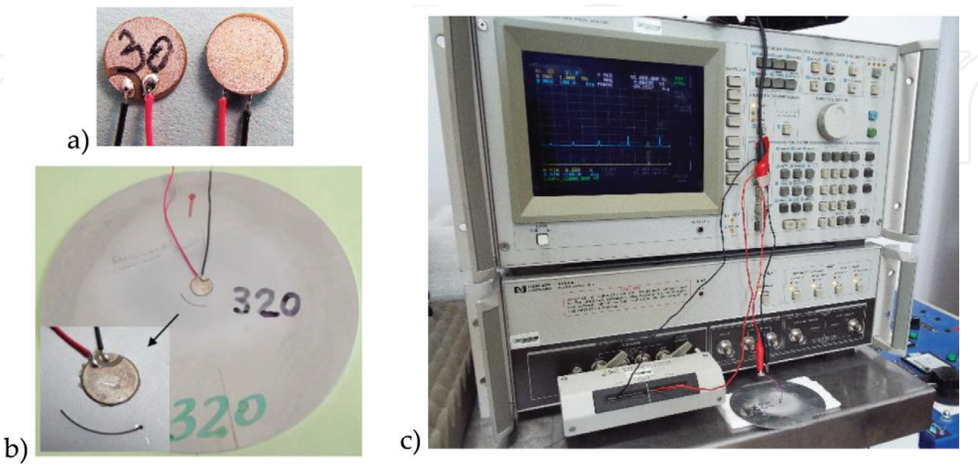

Figure 2. (a) PWAS STEMiNC type SMD 07T02R412WL; (b) DS with simulated damage at 7 mm from the PWAS; and (c) experimental set-up for EMIS recording at RT using the HP 4194A impedance analyzer.

http://dx.doi.org/10.5772/intechopen.78034

The saying "there is nothing more practical than a good theory" is widely known. In a complex tests program with the primary focus of the experiment, it was important to know well the theoretical tools. Indeed, the experiments were based on the concept of EMIS signature, so it was also important to master the theoretical basis of the EMIS method. The graphs summarized in this chapter, to which can be added the numerical analysis in [13, 14] and [29], as well as data, are given in **Table 1**; show that this goal has been met. Detailed analytical solutions are presented in [11–13]. Numerical calculations and experimental validation are widely described in [13, 6, 25, 29]. We cannot fail to notice the excellent monographs [30, 12] that guided the studies and experiments presented in this chapter. As a theoretical foundation, we retain the following equations that provide frequencies of flexural (*f*-indexed) and, respectively, axial (*a*-indexed) modes of a circular pristine disc:

$$\frac{\lambda^2 J_0(\lambda) + (1-v)\lambda J_0'(\lambda)}{\lambda^2 I_0(\lambda) - (1-v)\lambda I_0'(\lambda)} = \frac{J_0'(\lambda)}{I_0'(\lambda)}, \quad \omega_{j,f} := \lambda_{j,f}^2 \sqrt{\frac{D}{\rho h a^4}}, \quad D := \frac{Eh^3}{12(1-v^2)}$$
$$zJ_0(z) - (1-\nu)J_1(z) = 0, \quad z := \gamma a, \quad \omega_j := c_L(z)_{j,a}/a, \qquad c_L^2 := E/\left(\rho\left(1-v^2\right)\right) \tag{1}$$

The characteristic Eqs. (1) are obtained as solutions of the equation of motion for the transverse displacement w of a plate [30]:

$$D\nabla^4 w + \rho h \frac{\partial^2 w}{\partial t^2} = 0, \quad D := \frac{Eh^3}{12(1-v^2)} \tag{2}$$

$\nabla^4 = \nabla^2\nabla^2$, where ∇^2 is the Laplace operator. The Eqs. (1) give natural frequencies ω_j associated with solutions (eigenvalues) λ_j or z γ is wavenumber, $\gamma = \omega/c_L$. $J_0(\lambda)$ is the Bessel function of first kind and order zero, whereas $I_0(\lambda)$ is the modified Bessel function of first kind and order zero. D is the transverse (flexural) rigidity, E is Young's modulus, h is the plate thickness, a is the plate radius, v is Poisson's ratio, and ρ is mass density per unit area of the plate. As already mentioned, the DS were fabricated from A2024 aluminum alloy with a diameter of 2a=100 mm and a thickness of h =0.8 mm. The properties of the A2024 aluminum plates were: E= 73.146 MPa, ρ = 2780 kg/m^3, and ν = 0.3312. The frequencies values obtained by the experimental method are closer to the theoretical ones. The axial frequencies were noted with an italic font.

Hence, finally electromechanical impedance Z(ω) of a PWAS transducer bonded to disc specimen is:

ν_{th} (kHz)	12.57	19.69	28.38		*35.67*	38.63		50.51	63.95	78.97		*93.95*	95.57	
ν_{exp1} (kHz)	12.48	19.46	28.23		*35.89*	38.51		50.01	62.90	77.02		*92.04*	93.85	
ν_{exp2} (kHz)	12.65	19.91	28.27	28.63	*35.42*	37.35	38.07	38.87	49.32	50.53	63.62	77.93	*90.63*	93.73

Table 1. Theoretical (ν_{th}) and measured frequencies on pristine specimen (noted with ν_{exp1}) and on the arc at 15 mm damaged specimen (ν_{exp2}).

$$Z(\omega) = \frac{1}{i\omega C\left(1-k_p^2\right)}\left\{\left[1+\frac{k_p^2}{1-k_p^2}\frac{(1+v_a)J_1(\varphi_a)}{\varphi_a J_0(\varphi_a)-(1-v_a)J_1(\varphi_a)-\frac{a}{r_a}\chi(\omega)(1+v_a)J_1(\varphi_a)}\right]\right\}^{-1}$$
$$k_p^2 := \frac{2d_{31}^2}{s_{11}^E(1-v_a)\varepsilon_{33}^E},\ \varphi_a = \frac{\omega r_a}{c_P},\ c_P := \sqrt{\frac{1}{\rho s_{11}^E\left(1-v_a^2\right)}},\ \ \chi(\omega) = k_{str}(\omega)/k_{PWAS} \tag{3}$$

$k_{str}(\omega)$ is the dynamic stiffness of PWAS bonded on disc specimen; $k_{PWAS} = t_a/\left[r_a s_{11}^E(1-v_a)\right]$ is the PWAS stiffness; k_P is the planar coupling factor; c_P is the sound speed in PWAS disc; $c_L$is the longitudinal wave speed in disc specimen; v_a, r_a, and h_a are corresponding parameters of PWAS. Finally, s_{11}^E, ε_{33}^E, and d_{31} are recognized as PWAS compliance coefficient, dielectric permittivity and, respectively, strain constant.

The issues raised above are primarily qualitative, but at the same time, together with the results of numerical integration and with the measurements made on specimens, will show the capability and resources of the PWAS EMIS SHM technique. For example, spectrum splitting around resonance nominal frequencies of the pristine structure can be considered as an indication of the occurrence of mechanical damage in the monitored structure (**Figure 3**).

The numerical model used in tests program is based on the finite element method (FEM). FEM analysis allowed the study of damaged DSs [13, 14]. There was a good correlation between the analytical method and the experimental method.

The EMIS signature is calculated analytically (for regular geometric shapes, such as discs) and numerically. **Table 1** shows the theoretical natural frequencies described by the analytical model (1), the measured ones corresponding to the pristine DS (noted with ν_{exp1}) and to the "arc at 45 mm from PWAS" damaged DS (ν_{exp2}).

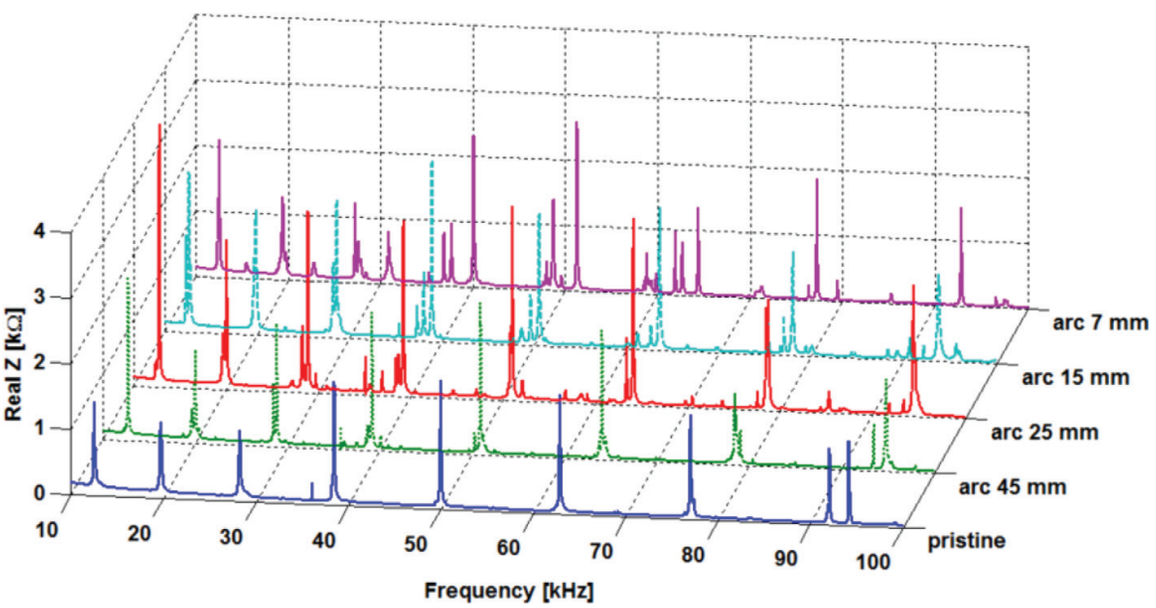

Figure 3. Measurement records for pristine specimen versus damaged one. Changes in RT EMIS signatures for different crack locations.

http://dx.doi.org/10.5772/intechopen.78034

Relationship (3) is an analytical one. The analytical results are compared with the experimental ones. The statistics of the analytical determinations and the measurements are based on an indicator. In statistics framework, the most available definitions of damages "metrics" could be: "root mean square deviation" (RMSD), mean absolute percentage deviation (MAPD), and "correlation coefficient deviation" (CCD). Expressions of such sizes given in terms of the real part of the impedance, Re (Z), are the following:

$$MAPD = \sum_N \left| \left[\mathrm{Re}(Z_i) - \mathrm{Re}\left(Z_i^0\right) \right] / \mathrm{Re}\left(Z_i^0\right) \right|, RMSD = \sqrt{\sum_N \left[\mathrm{Re}(Z_i) - \mathrm{Re}\left(Z_i^0\right) \right]^2 / \sum_N \left[\mathrm{Re}\left(Z_i^0\right) \right]^2}$$

$$CC = \frac{1}{\sigma_Z \sigma_{Z^0}} \sum_N \left[\mathrm{Re}(Z_i) - \mathrm{Re}\left(\overline{Z}\right) \right] \times \left[\mathrm{Re}\left(Z_i^0\right) - \mathrm{Re}\left(\overline{Z}^0\right) \right], CCD = 1 - CC \tag{4}$$

The symbols $\overline{Z}$ and Z^0 means averages in time and σ_Z and σ_{Z^0} represents the standard deviation. Herein, we are interested to "assess a RMS type damage metrics," both for the real fault embodied through cracks or cuts simulated on disk specimens, or to statistical evaluation of EMI changes caused by temperature or irradiation constraints on single PWAS, or DS, constraints generating so-called "virtual (or false) defects".

4. Checks before complex harsh environments tests

The test program started with the establishment of a reference database, with RT EMIS records and processing for each PWAS and DS. It is important to note that the recorded data has been analyzed even from the beginning taking into account the impact that a PWAS improperly glued on DS has on the EMIS graphs. **Figure 4** shows how an inappropriate bonding resulted in the specimen discredit.

Since the EMIS signature does not always clarify the origin of the damages – mechanical or electronic, generated by fatigue and the aging of the structure or by deficiencies of sensors bonding

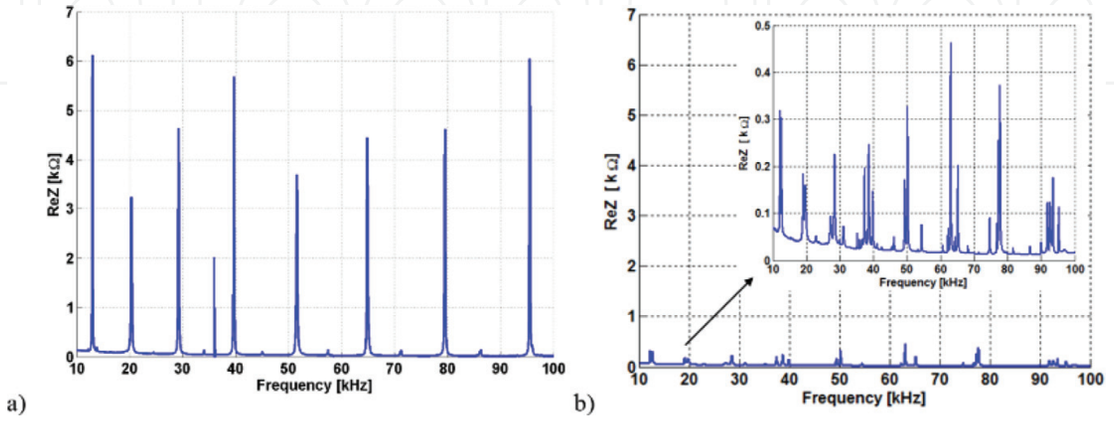

Figure 4. EMI signature for (a) a "good" bonding and (b) a "bad" bonding.

on the specimen and so on, special investigative means were added. This preliminary analysis is correlated with the experimental observation that there can be slight variation of EMIS for nominally identical specimens. It was considered that possible causes of EMIS signature changes were (a) fatigue and aging of the mechanical structure due to vibration, (b) unfulfillment of an adequate bonding of PWAS to the specimen, and (c) damage of PWAS itself.

Figure 5 top shows images obtained with *SAM 300*, at investigating the DS 122, particularly chosen wrong, for study. One can see: cracks in PWAS (red circles) caused by unequal forces applied during the bonding process; a piece of PWAS is broken (green rectangle); areas without glue (yellow rhombs). Another device used was the *digital microscope VHX 5000*. The VHX is an all-in-one microscope that incorporates observation, image capture, and measurement capabilities. **Figure 5** bottom shows two images of the DS 106 obtained with this device. The picture on the right is an enlarged image of the left side; a crack is shown in PWAS.

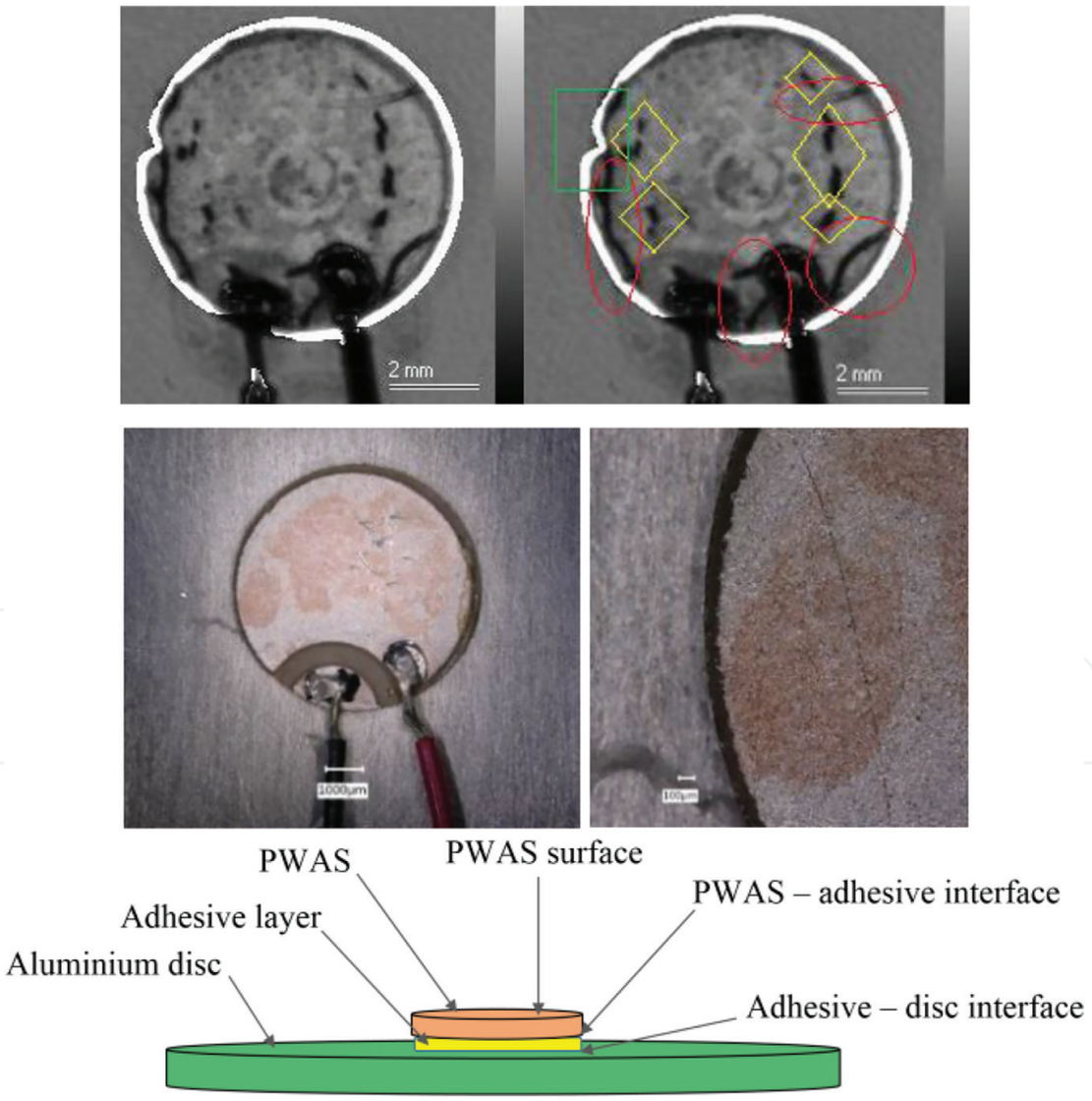

Figure 5. Top: Investigating the DS 122 with 300 scanning acoustic microscope (SAM); middle: Images obtained with digital microscope VHX 5000, DS106; and bottom: Areas of interest PWAS health monitoring.

http://dx.doi.org/10.5772/intechopen.78034

5. Describing tests protocol and results

5.1. The effects of the harsh environment on PWAS and DS EMIS signature

Two specimens exposed to harsh environmental conditions in the laboratory simulations are free PWAS sensors and circular plates with central bonded PWAS. EMIS was recorded both during exposure to harsh conditions, and in the intervals between these exposures, at RT, see **Table 2**. The technical details of the factors involved in one cycle of harsh environment exposure are presented in **Table 3**. The first stage of the complex test protocol stipulated five cycles of concomitant outer-space condition: high-temperature variation, radiation, and vacuum.

In the test program has been used special harsh environment simulation equipment, starting with the Dewar cryogenic vessel, and the convection oven with the Memmert UFE 400 digital temperature controller. Also, some of the experiments at negative temperatures were performed at INCAS in the environmental chamber INSTRON 5982, and the high temperatures in the thermostatic chamber FD 115 Binder.

The test program also developed experiments at the Horia Hulubei national institute for R and D in physics and nuclear engineering-IFIN-HH, in the gamma irradiation chamber 5000 with 60-Co circular distributed sources. The details are presented in the paper [26]. The measured radiation flow was 4.7 kGy/h. Five consecutive test cycles (**Table 3**) were programmed to provide a full irradiation dose of 23.5 kGy. The premise of the calculations was as follows: (a) the estimated

Tested specimen	Activity	Amount	Working time [h]
PWAS	EMI measuring at RT	30	20
	testing in harsh, space type, conditions	30	200
	EMI measurement after returning to RT	30	20
	EMI changes analysis	30	100
Disc with PWAS	EMI measuring at room temperature	34	20
	testing in harsh, space type, conditions	34	200
	EMI measurement after returning to RT	34	20
	EMI changes analysis	34	100

Table 2. Complex testing protocol for simulation of harsh space type conditions - first stage of complex tests.

Duration	Temperature (°C)	Vacuum (Pa)	Dose per step (kGy)	Dose per cycle (kGy)
Initial EMIS reading – RT				
0.5 h	−196	$1–10^{-2}$	2.35	4.7
1.0 h	RT	—	—	
0.5 h	+100	$1–10^{-2}$	2.35	
EMIS reading after each cycle – RT				

Table 3. Overview of one test cycle of cumulative environmental factors: Radiation, temperature, and vacuum tests.

complete dose for a mission on Mars is 110 mGy/year, which means a dose of about 15 μGy/h; (b) the highest absorbed doses determined by the Pioneer probes 10 and 11 were 15 kGy, and 4.3 kGy, respectively. Consequently, the dose rate determined by the gamma 5000 irradiation chamber has been considered as acceptable. The absorbed dose of 23.5 kGy corresponded to 5 h exposure at the measured dose of 4.7 kGy/h. The usual vacuum in the outer space is 10^{-14} Pa. Vacuum pressures below 10^{-1} Pa were obtained by using a tritium manifold, a high-vacuum plant containing a vacuum pump type TSH-171E Pfeiffer, and pressure vacuum controllers type TPG 262 Pfeiffer.

A reference database is created at the beginning of the tests; for example, see **Figure 6**. The strategy of the program was that, in the first stage of tests, the PWASs and DSs were tested using simultaneous environmental factors that are specific to outer space, see **Figure 7**, the case of disc specimen 127 [25]. Then, to characterize the influence of each factor on the EMIS signature, in the second phase the tests were developed with harsh environmental factors acting successively instead of simultaneously [28], see **Table 4**.

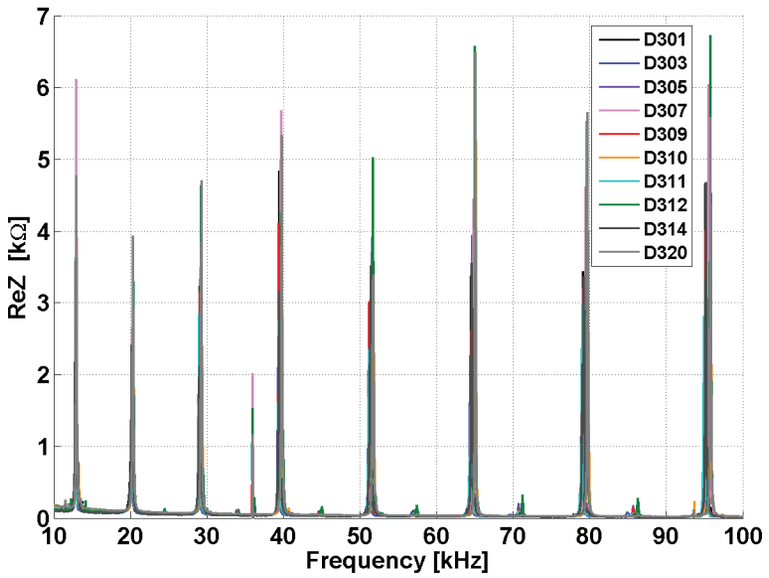

Figure 6. The experimental reference RT for the EMIS method: The signature of the health status of the structure.

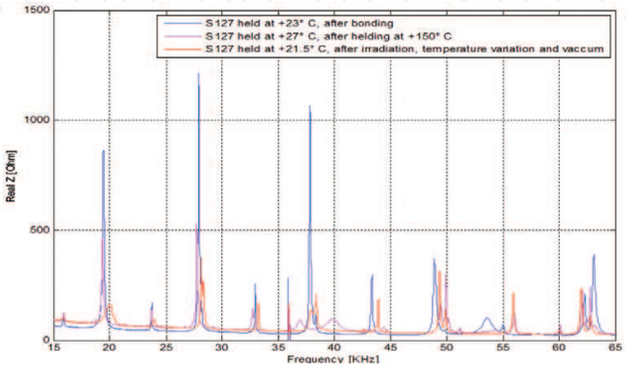

Figure 7. Summary of EMI measurements on S127 disc specimen, without simulated crack.

http://dx.doi.org/10.5772/intechopen.78034

The effects of harsh environment on PWAS. After performing the tests according to the protocols in **Tables 2** and **3**, it is noted that the resonance frequencies on the EMIS PWAS graphs are constantly moving from left to right when temperatures drop from high (+150°C) to cryogenic values (−70°C), as shown in **Figure 8a**. After completion of the tests at extreme temperatures, measurements were again made at RT.

A compensation technique [26, 28], in fact, a horizontal displacement of graphs, was used to obtain graphs in **Figure 8b**. As far as irradiations are concerned, they cause insignificant changes to EMIS signatures (**Figure 8c**). Thus, we can conclude that EMIS signature changes caused by environmental factors are reversible and consequently do not characterize real damage. The real damages are those of mechanical origin, which produce irreversible changes to the EMIS signature.

The effects on pristine DS. The EMIS behavior at extreme temperatures was analyzed on a set of 4 DS. Initially, the EMIS graph at RT (+25°C) was recorded. Next, tests at low temperatures,

#	Piezoelectric wafer active sensors (PWAS)	Disc specimens (DS)
1	Initial RT EMIS recording of 38 PWAS (26 of them was bonded on the aluminum disc)	Initial RT EMIS recording of 26 DS; 10 of them was eliminated
2	Tests and EMIS recording at high temperatures for 5 PWAS: +50/+200°C, step: +25°C	Fabrication of arc type mechanical damages (MD): arc at 45 mm (2 DS), 25 mm (3 DS), 15 mm (3 DS), and 7 mm (2 DS)
3	RT EMIS recording after high temperatures	RT EMIS recording after MD fabrication
4	Tests and EMIS recording at low temperatures for 5 PWAS: −25, −50, −70°C	Tests and EMIS recording at low temperatures for 4 DS: 0, −25, −50, −70°C
5	RT EMI recording after low temperatures	RT EMI recording after low temperatures
6	Tests and EMIS recording at high temperatures for 5 PWAS: +50/+150°C, step: +25°C	Tests and EMIS recording at high temperatures for 4 DS: +50, +75, +100, +125, and +150°C
7	RT EMIS recording after high temperatures	RT EMIS recording after high temperatures
8	Irradiation tests and EMIS recording for 2 PWAS at 3.71 Gy/h	Irradiation tests and EMIS recording for 2 DS at 3.71 Gy/h
9	RT EMIS recording after irradiation	RT EMIS recording after irradiation

Table 4. Tests summary – Second stage of complex tests.

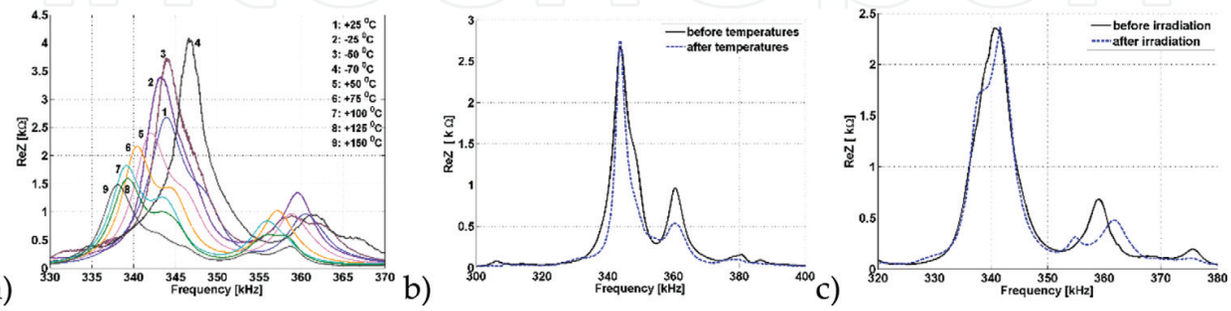

Figure 8. EMIS PWAS signatures: (a) synoptic graph of temperature cycling; (b) initial and after temperature cycling, both at RT, compensated values; and (c) initial and after irradiation tests, both at RT.

0, −25, −50, and −70°C were performed. When returning at the RT, T_1, (+22.4°C), it is noticed that the EMIS chart overlaps the initial one. After that, experiments at high temperatures up to +150°C, with a chosen step of 25°C, followed. When DS is brought to RT, T_2 (+23.6°C), it can be seen that EMIS returns to its original form, see **Figure 9a**.

Results similar to those of the PWAS case were also obtained in the case of 2 DS. The measurements were performed according to protocols before irradiation, during irradiation and after irradiation at RT, with the conclusion that the radiation does not produce splittings of the resonance peaks, but only negligible displacements of the peaks (**Figure 9b**), of the order of dozens of ohms.

5.2. The effects of the mechanical damages on PWAS and DS EMIS signature

Mechanical damages affect the EMIS signature in a well-defined way, namely causing the resonance peaks to split. This phenomenon intensifies in direct proportion to the decrease in distance from the PWAS center. Harsh environmental factors produce only displacements of resonance peaks and variations of amplitude on the EMIS signature, all practically reversible. (**Figure 3**).

The EMIS graphs in **Figure 10a** show, by comparison with the graph in **Figure 10b**, and the impact of the damages on the spectrogram. Of course, this impact is more pronounced when the damage is closer to the PWAS center and is manifested mainly as splittings of resonance peaks in new peaks. This observation generated the idea of developing a method of identifying mechanical damage as well as of dissociating the mechanical damage from the so-called false damage, that induced by environmental factors [31].

Therefore, based on experimental observations, the splitting of resonance peaks on the EMIS signature will be associated with the occurrence of a mechanical deterioration. Instead, the effects of harsh environmental conditions are limited only to reversible movements of resonance peaks with amplitude changes; if the temperatures do not exceed certain limits, the amplitudes are practically reversible, and returning to EMIS signatures in the case of RT. More insignificant are the modifications made on the EMIS graphs by irradiation specific to outer space.

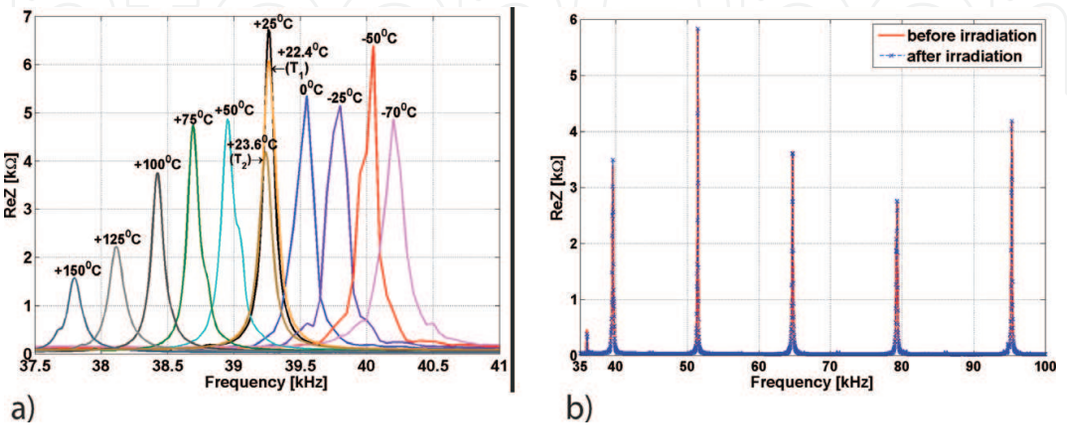

Figure 9. EMIS signature changes for a DS due to: (a) temperatures cycling; (b) irradiation.

http://dx.doi.org/10.5772/intechopen.78034

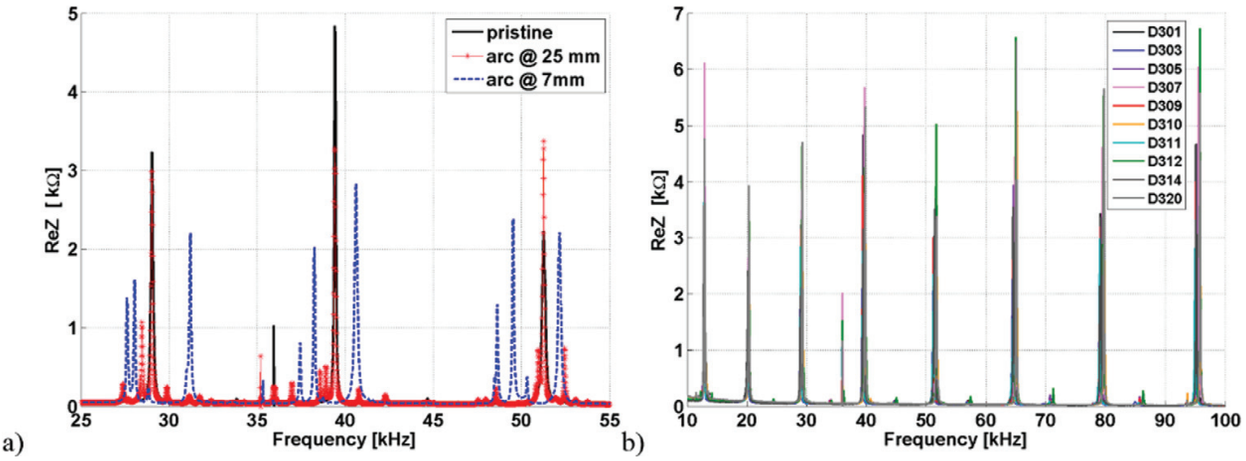

Figure 10. (a) Changes in EMIS signature, without damage versus damage (at 7 and 25 mm); (b) EMIS signature remains unchanged for different DS without damage.

A major tests result to propose a new, simple and effective approach to identifying mechanical damage. This approach allows the algorithmic distinction between real, mechanical damage and false damage, and caused by the harsh environmental factors.

5.3. Entropy method for damage detection and prediction

Figure 11 shows one of the multiple recordings done in the time domain with SLDV. The DS 138, without damage and with arc type defect at 15 mm, is scanned at a frequency of 78.4 Hz, see a 2D and a 3D representation. The position of the laser-cut slit is marked as a red peak. The displacement is given in nanometers depending on time [ms] (vibration measured in the *z*-direction, perpendicular to the disc, takes also negative values). The graph refers to a vibration of a specific point on the surface of the disk otherwise indicated in the picture. It can be seen that the concentric circles are uniformly distributed on the surface of the plate when there is no damage to disturb the wave propagation. In the case with the laser made damage, the amplitudes of the waves in the vicinity of the fabricated crack are much higher than all the other points of the disk producing distinct peak in the EMIS signature. **Figure 12** shows the use of SLDV for records in the frequency domain. For the same DS 138, a 3D image of the vibration at a frequency of 49.56 kHz is shown.

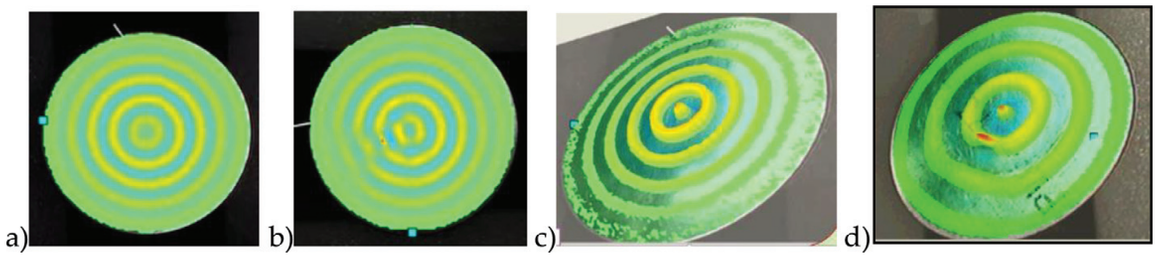

Figure 11. Recordings in time domain done with SLDV on DS 138: (a)disc without damage 2D representation; (b) DS with arc type defect at 15 mm—2D; (c) disc without damage 3D; and (d) DS with arc type defect at 15 mm—3D.

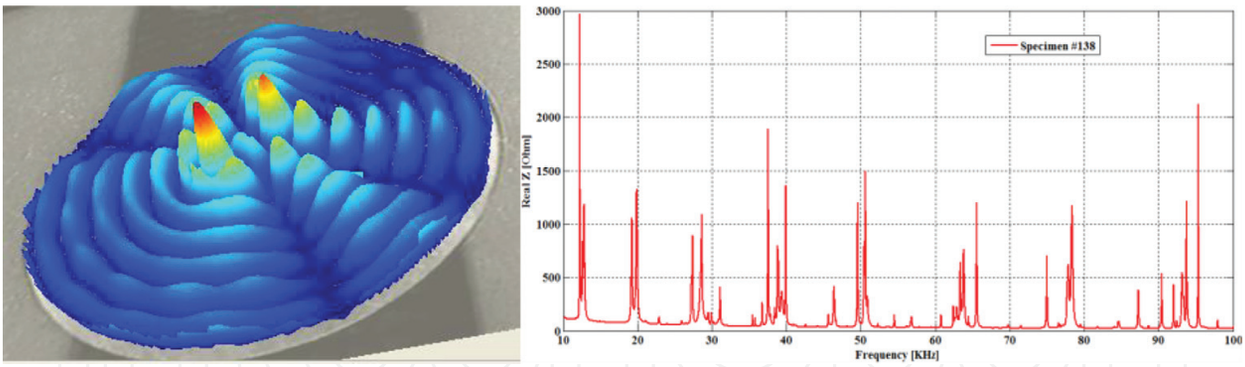

Figure 12. Recordings in frequency domain done with SLDV on DS 138 with mechanical damage; next is given the EMI signature of the disk.

The pattern of vibration in the presence and in the vicinity of the crack shows clear disorder. From here and from the paper [31] came the idea of exploiting the entropy concept in identifying the damage. Thus, an entropy method for damage detection and the prediction was proposed [28, 32]. Since the possible use of SLDV is very costly, we propose a simple method that uses the EMIS global signature. The proposed method can successfully substitute a possible but very expensive use of SLDV that should provide mode shapes for obtaining the global EMIS signature.

Consider the discretized system $Re(Z(\omega_i)) := R_i$, $\omega_i \in [\omega_a, \omega_b]$, $R_i \geq 0, i = 1, \ldots, n$ described by the probabilities $P = (p_1, p_2, \ldots, p_n)$. The complex information contained in EMIS signature measurements, respectively, in $Re(Z(\omega))$ data, is firstly processed in sizes assimilable as probabilities, $p_i \geq 0$, $i = 1, \ldots, n$ and $\sum_{i=1}^{n} p_i = 1$

$$p_i := \frac{Re(Z(\omega_i))}{\sum_{i=1}^{n} Re(Z(\omega_i))} := \frac{R_i}{C} \tag{5}$$

The normalized entropy of the set P is measured as:

$$H(P) = -\frac{\sum_{i=1}^{n} p_i \log_2 p_i}{\log_2 n} \tag{6}$$

The disorder produced in EMIS signature by the mechanical damage will be analyzed based on the investigative capacity of PWAS. This can be deducted from graphs recorded in **Figure 3**, where we find the EMIS signatures of undamaged DS, noted "u," of the DS in which the damage is located at the distance d_1 = 45 mm, noted "d_1", and so on, for the DS "d_2", "d_3", "d_4". This calculation is carried out on frequency intervals $\left[\omega_{a_j}, \omega_{b_j}\right]$, where certain resonance frequencies are present. Define

$$H(P, uu) = -\frac{\sum_{i=1}^{n} p_i \log_2 p_i}{\log_2 n} = -\frac{\sum_{i=1}^{n} \frac{2R_i^u}{2C^u} \log_2 \frac{2R_i^u}{2C^u}}{\log_2 n}$$

$$H(P, uu) = -\frac{1}{\log_2 n}\left[\frac{R_1^u}{C^u}\left(\log_2 R_1^u - \log_2 C^u\right) - \frac{R_2^u}{C^u}\left(\log_2 R_2^u - \log_2 C^u\right) - \ldots - \frac{R_n^u}{C^u}\left(\log_2 R_n^u - \log_2 C^u\right)\right] \tag{7}$$

$$H(P, uu) = -\frac{1}{C^u \log_2 n}\left(\sum_{i=1}^{n} R_i^u \log_2 R_i^u - C^u \log_2 C^u\right)$$

$$C^u := \sum_{i=1}^{n} R_i^u \tag{8}$$

$$p_{i,ud_k} = \frac{R_i^u + R_i^{d_k}}{\sum_{i=1}^{n}\left(R_i^u + R_i^{d_k}\right)} := \frac{R_i^u + R_i^{d_k}}{C^u + C^{d_k}} \tag{9}$$

$$C^{d_k} := \sum_{i=1}^{n} R_i^{d_k} \tag{10}$$

$$\begin{aligned} H(P, ud_k) &= -\frac{1}{\log_2 n}\left[\sum_{i=1}^{n}\frac{R_i^u + R_i^{d_k}}{C^u + C^{d_1}}\left(\log_2\left(R_i^u + R_i^{d_k}\right) - \log_2\left(C^u + C^{d_k}\right)\right)\right] \\ H(P, ud_k) &= -\frac{1}{\left(C^u + C^{d_k}\right)\log_2 n}\left[\left(\sum_{i=1}^{n}\left(R_i^u + R_i^{d_k}\right)\log_2\left(R_i^u + R_i^{d_k}\right)\right) - \left(C^u + C^{d_k}\right)\log_2\left(C^u + C^{d_k}\right)\right] \end{aligned} \tag{11}$$

The relationship (7) gives the entropy, or complexity, or the disorder modifications on the EMIS signatures, of the undamaged u DS in relation with himself, in short uu. We continue with the increased entropy ud_1 of damaged DS having the damage at a distance 45 mm, d_1, versus undamaged u DS, and so on up to ud_4 (**Table 5**).

From exploring the results in **Table 5**, it is noticeable that the PWAS active sensor senses the disorder caused by damage with satisfactory efficiency if this damage is located at a distance close to the sensor center, in this case at distances of 15–7 mm. This conclusion is useful for the

Frequency (kHz)	n for summation	uu	ud_1	ud_2	ud_3	ud_4	Averaged entropy ud_3 + ud_4 increasing vs. uu
26–32	601	0.826	0.850	0.851	0.904	0.905	0.079
36–42.5	651	0.771	0.821	0.805	0.882	0.876	0.108
47–53	601	0.821	0.819	0.830	0.880	0.904	0.071
58–68	1001	0.774	0.811	0.798	0.855	0.882	0.095
78–81.5	551	0.762	0.804	0.811	0.884	0.830	0.095
92.5–98.5	601	0.714	0.799	0.790	0.829	0.833	0.117

Table 5. Entropy values for disc specimens DS: u vs. u (uu), u vs. d_1 (ud_1), …, u vs. d_4 (ud_4) [28].

Frequency (kHz)	n for summation	Before irradiation	During irradiation	Entropy increasing
28–31	121	0.7601	0.7602	0.0001
38–41	121	0.7571	0.7576	0.0005
50–53	121	0.6721	0.6783	0.0062
63–67	121	0.7275	0.7295	0.0020
78–81.5	121	0.7437	0.7450	0.0013
93–97	121	0.7173	0.7183	0.0010

Table 6. Influence of radiations on EMIS signature, type "u" DS [28].

Frequency [kHz]	n for summation	RT	150°C	Entropy increasing
27–30	301	0.754	0.771	0.017
36.5–39.5	301	0.759	0.764	0.005
48–51.5	351	0.808	0.809	0.001
60.5–64.5	401	0.779	0.779	0.000
74–79	501	0.715	0.728	0.013

Table 7. Influence of temperature (after compensation) on EMIS signature, type "*u*" DS [28].

implementation of a SHM system, which should ensure an optimized distribution of monitoring sensors on the surface of the structure.

The fact that irradiation taken separately produces an insignificant change in the EMIS signature is attested in **Table 6**. If a compensation technique is considered and applied as in [26], the same conclusion applies to extreme temperature tests, see **Table 7**.

6. Conclusions

A first conclusion of descriptions and analysis made in this book chapter is that the cumulative impact of severe conditions of temperature and radiation has not generated decommissioning of PWAS sensors, thus confirming the survivability and sustainability of EMIS PWAS based SHM technology, as the first step towards de space vehicles transfer.

A second conclusion is that the splitting phenomenon of resonance peaks on EMIS signature can be associated with the occurrence of mechanical damage, making possible the clear dissociation of the changes determined by the harsh environmental conditions (temperatures and radiations). They are reduced mainly to reversible displacements of the resonance frequencies, with resonance amplitudes modifications, but if the temperatures do not cross certain limits, the amplitudes and frequencies return to those of RT case. Regarding radiations, they do not affect the EMIS graph.

Acknowledgements

The support from National Authority for Scientific Research and Innovation (ANCSI), for Star Space SHM project code ID 188/2012, and for NUCLEU Program project code 18-036/1 PN, "Complex mechatronic systems for procedures of launching systems recovery with active structural health monitoring," is thankfully acknowledged. During these programs, a large amount of experimental data was obtained that ultimately grounded the results and conclusions presented above.

Finally, we express our gratitude to Dr. Cristian Postolache from Horia Hulubei National Institute for R and D in Physics and Nuclear Engineering-IFIN-HH, Bucharest, for developing

the irradiation tests and to Dr. Cristian Rugina from Institute of Solid Mechanics of the Romanian Academy, Bucharest, for FEM applied to DS.

Conflict of interest

The authors declare that they have no conflict of interest.

Author details

Ioan Ursu, Mihai Tudose and Daniela Enciu*

*Address all correspondence to: enciu.daniela@incas.ro

Department of Systems, INCAS – National Institute for Aerospace Research "Elie Carafoli", Bucharest, Romania

References

[1] Farrar CR, Worden K. An introduction to structural health monitoring. Philosophical Transactions of the Royal Society A. 2007;**365**:303-315

[2] Kinet D, Megret P, Goossen KW, Qiu L, Heider D, Caucheteur C. Fiber Bragg grating sensors toward structural health monitoring in composite materials: Challenges and solutions. Sensors. 2014;**14**:7394-7419

[3] Ferdinand P. The evolution of optical fiber sensors technologies during the 35 last year and their applications in structural health monitoring. In: 7th European Workshop on Structural Health Monitoring, La Cité, Nantes, France; July 8–11, 2014

[4] Zagrai A, Doyle D, Gigineishvili V, Brown J, Gardenier H, Arritt B. Piezolectric wafer active sensor structural health monitoring of space structures. Journal of Intelligent Material Systems and Structures. 2010;**21**:921-940

[5] Ursu I, Giurgiutiu V, Toader A. Towards spacecraft applications of structural health monitoring. INCAS Bulletin. 2012;**4**(4):111-124

[6] Toader A, Ursu I, Enciu D. New advances in space SHM project. INCAS Bulletin. 2015; **7**(1):65-80

[7] Caimmi F, Bruggi M, Mariani S, Bendiscioli P. Towards the development of a MEMS-based health monitoring system for lightweight structures. In: International Electronic Conference on Sensors and Applications; 1–16 June, 2014

[8] Lynch JP, Loh KJ. A summary review of wireless sensors and sensor networks for structural health monitoring. The Shock and Vibration Digest. 2006;**38**(2):91-128

[9] Fritzen C-P. Vibration-based structural health monitoring - concepts and applications. Key Engineering Materials. 2005;**293-294**:3-20

[10] Liang C, Sun FP, Rogers CA. Coupled electro-mechanical analysis of adaptive material system – Determination of the actuator power consumption and system energy transfer. Journal of Intelligent Material Systems and Structures. 1994;**5**:12-20

[11] Zagrai A, Giurgiutiu V. Electro-mechanical impedance method for crack detection in thin plates. Journal of Intelligent Material Systems and Structures. 2001;**12**(10):709-718

[12] Giurgiutiu V. Structural Health Monitoring with Piezolectric Wafer Active Sensors. 2nd ed. Amsterdam: Elsevier Academic Press; 2014

[13] Rugina C, Toader A, Giurgiutiu V, Ursu I. The electromechanical impedance method for structural health monitoring of thin circular plates. Proceedings of the Romanian Academy, Series A, Mathematics, Physics, Technical Sciences, Information Sciences. 2014;**15**(3): 272-282

[14] Rugina C, Enciu D, Tudose M. Numerical and experimental study of circular disc electromechanical impedance spectroscopy signature changes due to structural damage and sensor degradation. Structural Health Monitoring - an International Journal. 2015;**14**(6): 663-681

[15] Keith Mobley R. An Introduction to Predictive Maintenance. 2nd ed. Amsterdam: Butterworth Heinemann (Elsevier); 2002

[16] Isermann R. Fault-diagnosis systems. Germany: Springer; 2006

[17] Speckmann H, Roesner H. Structural Health Monitoring: A Contribution to the Intelligent Aircraft Structure, ECNDT 2006 - Tu.1.1.1

[18] Peairs DM, Grisso B, Inman DJ, Page KR, Athman R, Margasahayam RN. Proof-of-concept application of impedance-based health monitoring on space shuttle ground structures. NASA-TM-2003-211193; 2003

[19] Mancini S, Tumino G, Gaudenzi P. Structural health monitoring for future space vehicles. Journal of Intelligent Material Systems and Structures. 2006;**17**:577-585

[20] Pisacane VL. The Space Environment and its Effects on Space Systems. Reston, VA: AIAA Education Series; 2008

[21] Giurgiutiu V, Lin B, Santoni-Bottai G, Cuc A. Space application of piezolectric wafer active sensors for structural health monitoring. Journal of Intelligent Material Systems and Structures. 2011;**22**(8):1359-1370

[22] Ramachandran V, Gadlage M, Ahlbin J, Narasimham B, Alles M, Reed RA, Bhuva B, Massengill L, Black J, Foster CN. Application of a novel test system to characterize single event effects at cryogenic temperatures. Solid State Electronics. 2010;**54**:1052-1059

[23] Nymmik R. Initial conditions for radiation analysis: Models of galactic cosmic rays and solar particle events. Advances in Space Research. 2006;**38**:1182-1190

[24] *** STAR project code ID 188/2012. Structural health monitoring in spacecraft structures using piezoelectric wafer active sensors (PWAS) multimodal guided waves. National Authority for Scientific Research—ANCS, UEFISCDI, STAR Programme

[25] Enciu D, Tudose M, Neculaescu B, Toader A, Ursu I. Damage identification and damage metrics in SHM. Proceedings of AEROSPATIAL 2014, Bucharest, 18–19 September. pp. 349-364. ISSN 2067–8614, 2014

[26] Ursu I, Enciu D, Toader A. Towards structural health monitoring of space vehicles. Aircraft Engineering and Aerospace Technology. 2017;**89**(6):920-927

[27] Ursu I, Toader A, Enciu D, Stefanescu DM. Advanced measurements in star space project on structural health monitoring. Proceedings of XXI IMEKO World Congress. 2015:2084-2087. ISSN 9781510812925

[28] Enciu D, Ursu I, Toader A. New results concerning SHM technology qualification for transfer on space vehicles, Structural Control and Health Monitoring. 2017;**24**(10):e1992. DOI: 10.1002/stc.1992

[29] Rugina C, Giurgiutiu V, Ursu I, Toader A. Finite element analysis of the electromechanical impedance method on aluminum plates in SHM. Proceedings of AEROSPATIAL 2014, Bucharest, 18–19 September, 2014:343-348. ISSN 2067–8614

[30] Leissa A. Vibration of Plates, NASA SP-160. US Gov't Printing Office; 1969

[31] Yang Z-B, Chen X-F, Xie Y, Zhang X-W. The hybrid multivariate analysis method for damage detection. Structural Control and Health Monitoring. 2016;**23**:123-143

[32] Enciu D, Ursu I, Tudose M. Complex method for online identification of mechanical damages using the electromechanical impedance spectroscopy, avoiding the false diagnosis. OSIM Patent no. RO131152B1/29.12.2017. Gold Medal and the Special Prize from the Turkish Patent and Trademark Office for the patent no. RO131152B1/29.12.2017 awarded at the 46th Edition of the International Invention Salon held at Geneva, Switzerland; 11–15 April, 2018

IntechOpen